Proceedings of FEDSM99
3rd ASME/JSME Joint Fluids Engineering Conference
July 18-23, 1999, San Francisco, California, USA

FEDSM99-7172

NUMERICAL SIMULATION OF FLOW PAST A SQUARE CYLINDER

Ahmad Sohankar
Thermo and Fluid Dynamics
Chalmers University of Technology
S-412 96 Göteborg
Sweden
Email: sohankar@tfd.chalmers.se

C. Norberg
Division of Heat Transfer
Lund Institute of Technology
Box 118, S-221 00 Lund
Sweden
Email: chris@ms.vok.lth.se

L. Davidson
Thermo and Fluid Dynamics
Chalmers University of Technology
S-412 96 Göteborg
Sweden
Email: lada@tfd.chalmers.se

ABSTRACT

2D and 3D unsteady flow past a rigid prism of a square cross-section with one side facing the oncoming flow is numerically simulated for Reynolds numbers between 200 to 500. An incompressible code is used employing an implicit fractional step method finite-volume with second-order accuracy in space and time. For 2D flow, it is found that, for $Re > 300$, the time-mean flow patterns are not perfectly symmetric with respect to the oncoming flow. In contrast, such a non-symmetric mean flow pattern is not observed in 3D simulations. There is a marked and characteristic pulsation in the force components in the 3D flow for $Re < 300$. These force pulsations contain characteristic time periods with high and low levels of forces. It is found that when the flow is within a low levels of forces the intensity of three-dimensional effects becomes stronger, whereas the opposite is true within a high level of forces.

INTRODUCTION

In the past, the flow around bluff bodies, such as circular and rectangular cylinders, has been extensively studied owing to its relevance to technical problems associated with energy conversion and structural design. Over the last twenty years, a vast amount of studies has been conducted to increase the understanding of different transition processes of the flow past a circular cylinder — experimentally, numerically and theoretically, for a review see Williamson (1996). By contrast, there are very few similar studies found on flow past rectangular cylindrical structures, e.g. the square cylinder, at moderate Reynolds numbers where a 2D/3D wake transition occurs. As an example, at Reynolds numbers less than about 500 there is only one single set of experiments reporting the influence of Reynolds number on the mean drag coefficient, see Okajima *et al.* (1995). Recently, two transition processes were numerically investigated by the present authors. First, in Sohankar *et al.* (1998), for a square cylinder at various angles of incidence, the onset of vortex shedding is investigated by using the Stuart-Landau equation and second, in Sohankar *et al.* (1999) the transitional 3D wake flow behind a square cylinder is studied. In the second work, it is found that a transition from 2D to 3D shedding flow between $Re = 150$ and $Re = 200$ occurs and that both spanwise instability modes, A and B, are present in the wake transitional process, similar to the flow around a circular cylinder. However, seemingly in contrast to a circular cylinder, the transitional flow around a square cylinder exhibits a phenomenon of distinct low frequency force pulsations ($Re = 200 - 300$) with period about 10–16 times the shedding period. Recently, force pulsations with a period of approximately 10 times the primary shedding period are also reported for a zero-thickness flat plate at $Re = 250$ by Najjar & Balachandar (1998).

In Sohankar *et al.* (1999), it is also shown that the Strouhal number and the mean drag coefficient for the 3D simulations are in general agreement with existing experiments. The 2D results for mean drag are in reasonable agreement with experiments, although other quantities and flow characteristics for $Re \geq 200$ are for the most part in sharp contrast with available experimental data and 3D results.

The main objectives of the present study were to further in-

vestigate 3D transitional features in the flow past a square cylinder and to make additional comparisons with 2D results at moderate Reynolds numbers, $Re = 200 - 500$.

Computational Details

The flow is described in a Cartesian coordinate system (x, y, z), in which the x-axis is aligned with the inlet flow direction, the z-axis is parallel with the cylinder axis and the y-axis is perpendicular to both directions, as shown in Fig. 1. A fixed two-dimensional square cylinder with a side d is exposed to a constant free stream velocity, U_∞. An incompressible flow with constant fluid properties is assumed. The Reynolds number is defined as $Re = U_\infty d/\nu$. All geometrical lengths are scaled with d. Scaling with d also applies to the Strouhal number, $St = f_S d/U_\infty$, where f_S is the shedding frequency, and for all forces. Velocities are also scaled with U_∞, and physical times with d/U_∞. In y-direction, the vertical distance between the upper and lower walls, H, defines the solid blockage of the confined flow (blockage parameter, $\beta = 1/H$).

An incompressible finite volume code, which is based on a fractional step technique, is used and employs a non-staggered grid arrangement. The scheme is implicit in time, and a second order Crank-Nicolson scheme is used. All terms are discretized using the second-order central differencing scheme. The time-marching calculations are started with the fluid at rest, and a constant time step $\Delta t = 0.025$ is used. The calculations are carried out for different resolutions, $169 \times 121 \times 25$ (3D simulation, $A = 6$), $169 \times 121 \times 41$ (3D simulation, $A = 10$), $209 \times 129 \times 41$ (3D simulation, fine resolution for $Re = 500$, $A = 6$) and 169×121 (2D simulations).

The following boundary conditions were used. A uniform flow was prescribed at the inlet, which is located X_u units upstream of the cylinder. At the outlet, located X_d units downstream of the cylinder, the convective boundary condition was used for all velocity components. No-slip conditions were prescribed at the body surfaces. Symmetry conditions simulating a frictionless wall were used at the upper and lower boundaries. A periodic boundary condition was used in the spanwise direction. The normal derivative for the pressure was set to zero at all boundaries. In the present study, X_u, X_d and H were set to 8.5, 12.5 and 18, respectively, see Fig. 1.

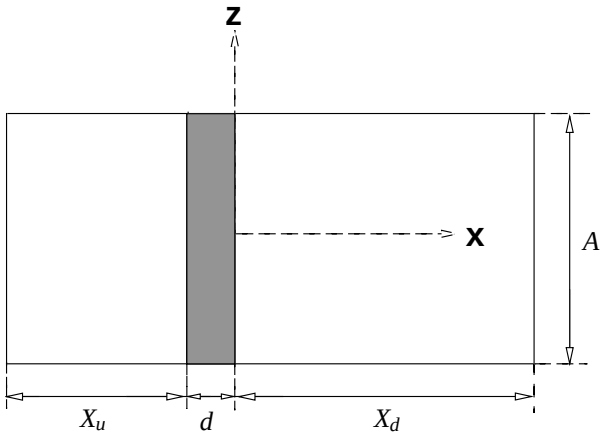

Figure 1. Flow configuration.

Re	LF/HF	$R_{\omega 1}$	$R_{\omega 2}$	$R_{\omega 3}$	$\omega 3$	$-C_{P3}$
200	LF	0.95	0.93	0.88	3.82	1.92
200	HF	0.99	0.99	0.96	3.54	1.04
250	LF	0.90	0.96	0.87	4.41	2.40
250	HF	0.99	0.98	0.92	3.28	1.70

Table 1. Summary of results taken from spanwise vorticity contours at minimum lift instances, $A = 6$, see e.g. Fig. 3. The ratio of spanwise vorticity (ω_z) and magnitude vorticity (ω=$\sqrt{{\omega_x}^2 + {\omega_y}^2 + {\omega_z}^2}$), R_ω, and pressure coefficient, C_P, are chosen at point where ω_z is extreme. Indexes 1-3 in this table refer to developing vortices from the upper side (black one), the lower side (white one) and detached vortex (white one) at the position of $x \approx 4 - 5$, respectively.

1 Wake Flow Transition

Within the early stages of the wake transition process ($Re = 200 - 250$) a marked and characteristic pulsation occurs in the force components, see Sohankar *et al.* (1999). Such a pulsation is seen in Fig. 2 for $Re = 200$ but is not observed for $Re = 500$. These force pulsations contain characteristic time periods with high and low levels of forces which are referred to as HF and LF regions, respectively. Associated with the presence of force pulsations, a time-shifted positive coupling is observed between the instantaneous shedding frequency and the lift amplitude, with shedding frequency leading the amplitude, see Sohankar *et al.* (1999). In the time regions of high force levels, the flow is in an ordered state with relatively small spanwise variations, whereas the three-dimensional effects are strong in low force regions with a seemingly chaotic spanwise flow structure. The pulsating forces, especially the drag, are closely related to the activity of the secondary vortices, see Sohankar *et al.* (1999).

Here we try to expand this matter further by studying the vortex structure in HF and LF regions to find the main feature of the flow in these two regions. Spanwise vorticity contours in the mid-plane ($z = 0$) at the instance of minimum lift force for $Re = 250$ are shown in Fig. 3. In this figure and other figures

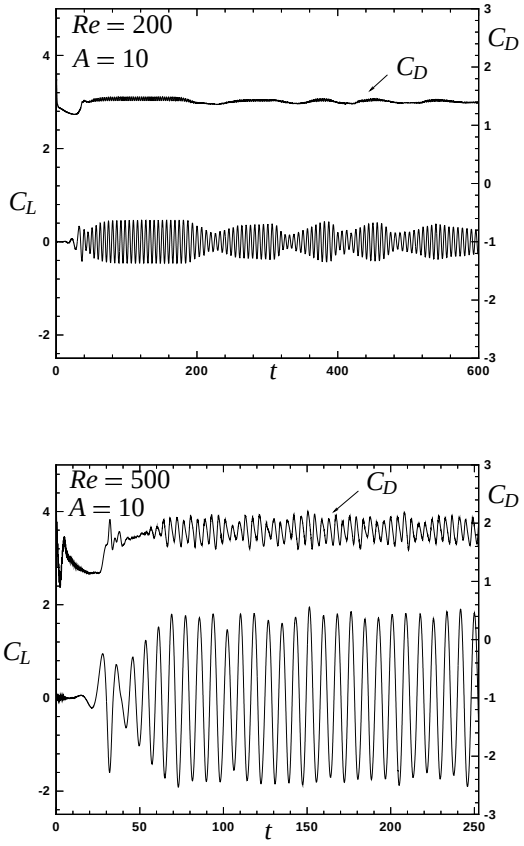

Figure 2. Time history of spanwise-averaged lift and drag coefficients (3D simulations, $A = 10$). Top: $Re = 200$ ($St = 0.160$, $C_D = 1.41$, $C_{D'} = 0.023$, $C_{L'} = 0.22$), bottom: $Re = 500$ ($St = 0.122$, $C_D = 1.87$, $C_{D'} = 0.148$, $C_{L'} = 1.25$).

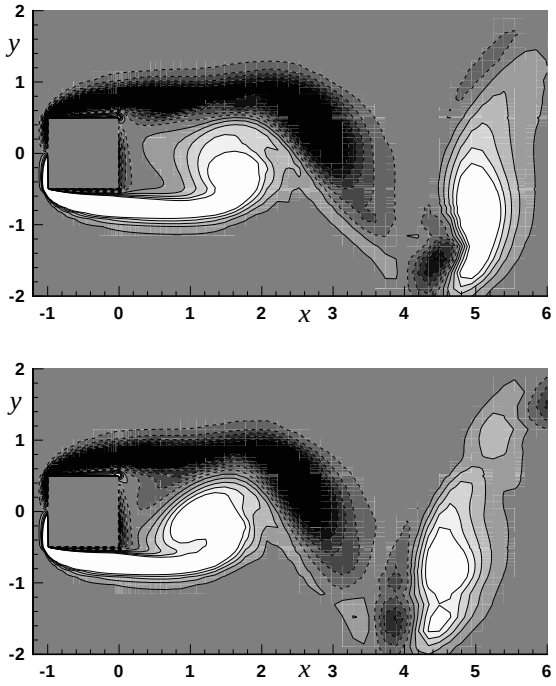

Figure 3. Spanwise vorticity contours in the plane $z = 0$ in the position of minimum lift force. (3D-simulations, $A = 6$, $Re = 250$). Top: LF region ($C_L = -0.26$); bottom: HF region ($C_L = -0.34$).

not shown here, it is observed that the shear layers developing from the upstream edges of the cylinder are not exactly similar in HF and LF regions. In the LF region, the free shear layers from the upper edge (black one in Fig. 3) are extended farther downstream in comparison to the case in the HF region, before rolling up to spanwise (von Kármán) vortices. In addition, in the HF region, the free shear layers from the lower edge (white one in Fig. 3) are rolled up closer to the cylinder than is the case in the LF region. Thus, in the HF region the first vortex is shed in the wake at a position closer to the body. This is also consistent with the fact that the frequency of vortex shedding is higher in the HF region than in the LF region. The higher frequency means that the process of spanwise vortex shedding is faster. Similar findings were reported by Najjar & Balachandar (1998) for flow past a normal plate. They found that the spanwise vortices in the HF region are more compact and roll up closer to the back side of the normal plate with significantly shorter mean recirculation region than is seen in the LF region.

Sohankar *et al.* (1999) report that the spanwise coupling of forces and the associated near-wake flow components were higher in HF regions than in LF regions. For example, it is shown that the spanwise variations of the sectional drag in the HF region are small in transition ($Re = 200$ and $Re = 250$), whereas the variations in the LF region are significantly higher. This means that the degree of three dimensionality is higher in the LF regions than in the HF regions. Further investigation using different components of vorticity also confirms this finding. Table 1 provides the ratio of spanwise to total vorticity at minimum lift instances R_ω ($=\omega_z/\sqrt{(\omega_x{}^2 + \omega_y{}^2 + \omega_z{}^2)}$), at the position of extreme ω_z in three positions in the wake region for $Re = 200$ and $Re = 250$. These three positions of extreme ω_z are located on the core of the developing vortices from the upper side (black one), the lower side (white one) and detached vortex (white one) at the position of $x \approx 4 - 5$, respectively, e.g see Fig 3. Similar results to those provided in Table 1, were also observed for the instant of maximum lift. From Table 1, it is seen that the R_ω has higher values (close to one) in HF regions than in LF regions for $Re = 200$ and $Re = 250$. High values of R_ω in the order of one mean that the magnitude of ω_z and ω are close or that the effect of two other

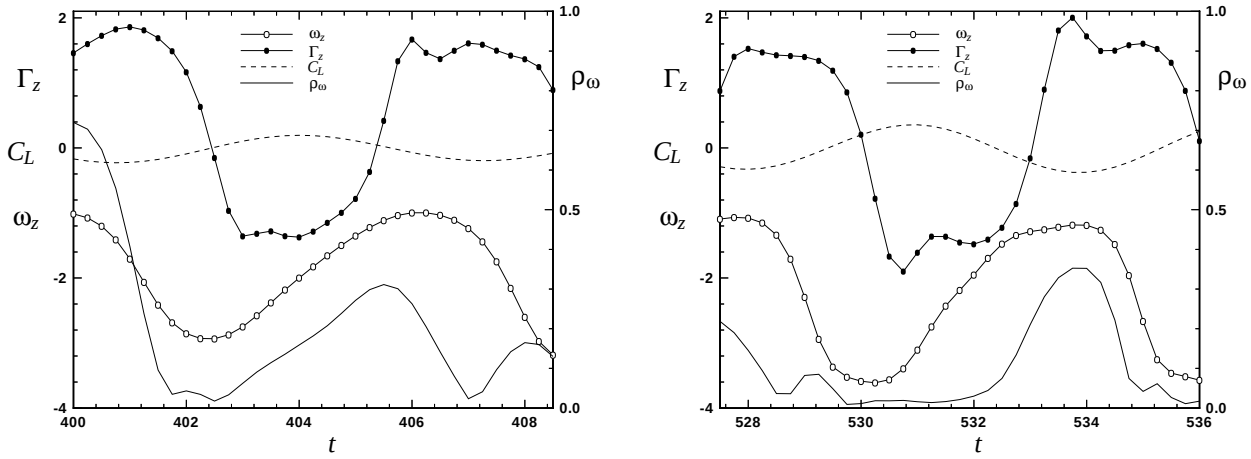

Figure 4. Spanwise circulation (Γ_z) in plane $z = 0$ together with spanwise-averaged lift coefficient, spanwise vorticity (ω_z) and vorticity ratio (ρ_ω=$\sqrt{\omega_x{}^2 + \omega_y{}^2}/\sqrt{\omega_x{}^2 + \omega_y{}^2 + \omega_z{}^2}$) *vs.* time for $Re = 200$, $A = 6$. left) LF region, right) HF region. The circulation is calculated in the domain $x \in (0,6)$, $y \in (-2,2)$. The ω_z and ρ_ω are taken from a point in the free shear layer at the location of $x = 1$, $y = 0.6$ and $z = 0$.

components, ω_y and ω_x, are negligible. Thus, the degree of two dimensionality is higher in HF regions than in LF regions.

It is important to mention that the corresponding values of peak vorticity, ω, and pressure coefficient, $-C_P$, at the center of the first detached vortex (e.g see Fig. 3 at the position of $x \approx 4-5$) in LF regions are higher than in HF regions, see Table 1. This means that more intense vortices (higher ω and $-C_P$ in the core of vortices) are generated in LF regions than in HF regions. In general, the level of spanwise vorticity in HF and LF regions is approximately similar, e.g. see Fig. 4. As a crude measure of the intensity of the Kármán vortices, the spanwise circulation, Γ_z, was calculated at mid-span ($z = 0$) in the region $y \in (-2,2)$, $x \in (0,6)$. In referring to this figure, for $Re = 200$, it can be noted that, in LF and HF regions, the time variations in the spanwise circulation, Γ_z, are approximately stable with regard to their amplitude and vary between the limits of ± 2 with a frequency corresponding to the lift signal. Such variations are also seen in this figure for spanwise vorticity, ω_z, at a selected point in the free shear layer ($x = 1$, $y = 0.6$, $z = 0$). In confirmation of this finding, it was also found that the spanwise circulation ratio, $\Gamma_{zHF}/\Gamma_{zLF}$, is 0.97 for the detached vortex at the position of $x \approx 4-5$ in the instance shown in Fig. 3. On the other hand, the strength of the streamwise vorticity becomes stronger in the LF region. As is seen, the level and variation of the vorticity ratio, ρ_ω (=$\sqrt{\omega_x{}^2 + \omega_y{}^2}/\sqrt{\omega_x{}^2 + \omega_y{}^2 + \omega_z{}^2}$), at a selected point in the free shear layer ($x = 1$, $y = 0.6$, $z = 0$) are higher in the LF region than in the HF region. It was observed that the intensity of the streamwise vorticity and the calculated streamwise circulation, Γ_x, in different streamwise (yz) planes were higher when the flow is in a LF region (these plots are not shown here, see Sohankar (1998)). Similar findings as for $Re = 200$ were also observed for $Re = 250$.

In general, referring to Figs. 3-4 and Table 1 and as well as other findings not reported here (see Sohankar (1998)), it is concluded when the flow is in a LF region the intensity of three-dimensional effects becomes stronger while the opposite is true in a HF region.

2 Comparison between 2D and 3D results

Sohankar *et al.* (1999) report that the 2D results for mean drag are in reasonable agreement with experiments, although other quantities for $Re \geq 200$ are for the most part in sharp contrast with available experimental data and the 3D results. Here, we try to make additional comparisons by comparing 2D and 3D flow characteristics.

Time averaged streamlines of 2D simulations for $Re = 300$ and $Re = 500$ and 3D simulation for $Re = 500$ ($A = 10$) are shown in Fig. 5. It was found that the time-mean flow patterns were perfectly symmetric for $Re \leq 300$ (Fig. 5, upper), whereas the flow patterns were not perfectly symmetric with respect to the oncoming flow for $Re = 400$ and $Re = 500$. This non-symmetric mean flow pattern in 2D simulations is shown in Fig. 5 (middle) for $Re = 500$. Such a non-symmetric mean flow pattern has also been reported by Breuer(1998) for 2D flow around a circular cylinder at $Re = 3900$. As is seen from Fig. 5 (lower) the 3D-simulated mean flow pattern is symmetric for $Re = 500$. As is observed in Fig.5, the mean flow pattern for 2D and 3D simulations at $Re = 500$ is approximately similar on the front, top and bottom sides of the cylinder, whereas there are many differences on the rear side where the wake flow develops. This difference is also clearly seen in Fig 6, which shows the pressure coefficient, C_P,

around the cylinder. On the basis of this figure, the differences in C_P for 2D and 3D simulations are smaller on the sides of the body then on the rear. In spite of the differences in the values of C_P on the rear side, the averaged value of C_P for 2D simulation on this side was the same as for 3D simulation. This is the reason why the drag coefficient for $Re = 500$ is in good agreement in 2D and 3D simulations (2D:$C_D = 1.90$, 3D:$C_D = 1.87$). When comparing averaged 3D results with 2D results for RMS drag, RMS lift, RMS base pressure coefficient and Strouhal number, the differences were about -63%, $+6\%$, -40% and -27%, respectively. For 2D flow, a non-zero mean lift was found for $Re > 300$. For instance, the time-mean lift coefficient for $Re = 400$ was equal to $C_L = -0.04$. There is also a significant difference between 2D and 3D simulations in pressure coefficient and streamwise velocity at the centerline, see Fig. 6. It is important to mention that the 2D time-averaged results did not change even when the averaging time was increased up to 50 shedding periods. In Sohankar *et al.* (1999) it is shown that the lift and drag spectra from 2D simulations for $Re > 300$ exhibit a scenario of period-doublings while there are no signs of such period-doublings in the 3D simulations, see Sohankar *et al.* (1999). In connection with period-doublings for $Re = 400, 500$, it is observed that there are two and four peaks in each main shedding period in the time history of the lift and drag forces, respectively, see Sohankar *et al.* (1999). Corresponding to these four peaks for drag, four vortices are shed during each period which lead to a sudden drop in the time history of the drag force between each two peaks. The intensity and the formation time of these vortices are different, which leads to different lift and drag force levels. For some reason one of these extra two vortices which are created during one main shedding period occurs more frequently on one side than on the other. By mutual interaction oppositely-signed vortices amalgamate together in the near wake with the strongest pair of such a cluster of two vortices having a preference to one of the side of the centerline, see Sohankar *et al.* (1999). This causes an asymmetric behavior in 2D simulations for $Re > 300$. It should be emphasized that the degree of asymmetry could be dependent of computational factors such as the computational domain size and the spatial/temporal resolution. Nevertheless, it is quite clear from the 3D simulations (Sohankar et al. 1999) and laboratory experiments (Okajima 1982) that the flow around a sufficiently long cylinder is inherently three-dimensional at these Reynolds numbers. Thus, it is expected that using 2D simulations of inherently 3D flow leads to a non-accurate prediction of the flow structures and global quantities because the structure of flow in the spanwise direction is completely eliminated.

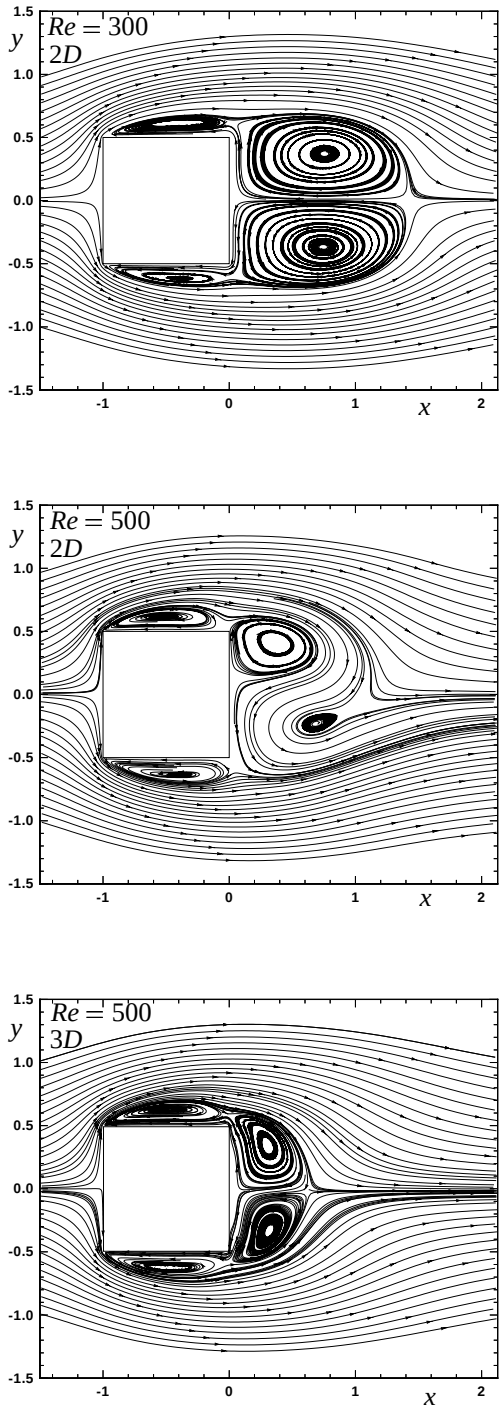

Figure 5. Time-averaged stream lines in 2D simulations for $Re = 300$ and $Re = 500$ and a 3D simulation for $Re = 500$ ($A = 10$).

Conclusions

Numerical simulations of unsteady 2D and 3D flow around a square cylinder at zero incidence are presented for $Re = 200 - 500$.

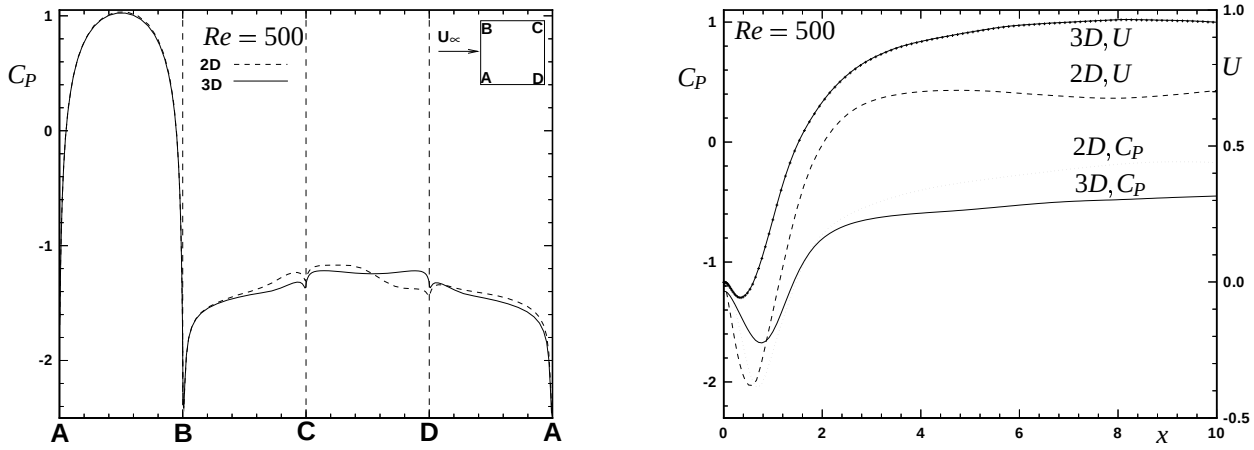

Figure 6. Comparison of 2D and 3D results for $Re = 500$. left) Time-averaged pressure coefficient around the cylinder; right) time-averaged pressure coefficient and streamwise velocity at the centerline.

For 2D flow, it is found that, for $Re > 300$, the time-mean flow patterns are not perfectly symmetric with respect to the oncoming flow. In contrast, a symmetric mean flow pattern is observed in 3D simulations. It is believed that the asymmetric behavior in 2D simulations for $Re > 300$ in some way is related to the scenario of period-doublings. The phenomenon of period-doubling is a dominant feature in the 2D simulations while there are no signs of such period doublings in the 3D-simulations. Thus, it is expected that using 2D simulations of inherently 3D flow leads to a non-accurate prediction of flow structures and global quantities because the structure of the flow in the spanwise direction is completely eliminated.

There is a marked and characteristic pulsation in the force components of three dimensional flow for $Re < 300$. These force pulsations contain characteristic time periods with high (HF) and low (LF) levels of forces. The central parts of the von Kármán vortices at instants just after they have been detached from the cylinder appears to be more intense in the LF region than in the HF region. The intensity in this context is based on the magnitude of the vorticity vector and the degree of pressure suction. The level of non-spanwise vorticity is higher when the flow is in a LF region, while the level of spanwise vorticity in HF and LF regions is approximately similar. Thus, it is concluded that the degree of two dimensionality is higher in HF regions, while the opposite is true in LF regions.

REFERENCES

Breuer, M. (1998). Large eddy simulation of the subcritical flow past a circular cylinder: numerical and modeling aspects. *Int. J. Num. Meth. Fluids 28*, 1281–1302.

Najjar, F. M. and S. Balachandar (1998). Low-frequency unsteadiness in the wake of a normal flat plate. *J. Fluid Mech. 370*, 101–147.

Okajima, A. (1982). Strouhal numbers of rectangular cylinders. *J. Fluid Mech. 123*, 379–398.

Okajima, A. (1995). Numerical analysis of the flow around an oscillating cylinder. In P. W. Bearman (Ed.), *Proc. 6th Int. Conf. Flow-Induced Vibration, London, UK, 10-12 April*, pp. 1–7. Balkema, Rotterdam.

Sohankar, A. (1998). *Numerical Study of Laminar, Transitional and Turbulent Flow Past Rectangular Cylinders*. Ph. D. thesis, Dept. of Thermo and Fluid Dynamics, Chalmers University of Technology, Gothenburg.

Sohankar, A., C. Norberg, and L. Davidson (1998). Low-Reynolds number flow around a square cylinder at incidence: Study of blockage, onset of vortex shedding and outlet boundary condition. *Int. J. Num. Meth. Fluids 26*, 39–56.

Sohankar, A., C. Norberg, and L. Davidson (1999). Simulation of three-dimensional flow around a square cylinder at moderate Reynolds numbers. *Phys. Fluids A 11*, 288–306.

Williamson, C. H. K. (1996). Vortex dynamics in the cylinder wake. *Ann. Rev. Fluid Mech. 28*, 477–539.